University of Plymouth

PEARL **https://pearl.plymouth.ac.uk**

Faculty of Science and Engineering School of Engineering, Computing and Mathematics

2021-06-22

Performance of a plate-wave energy converter integrated in a floating breakwater

Zheng, Siming

http://hdl.handle.net/10026.1/17217

10.1049/rpg2.12230
IET Renewable Power Generation
Institution of Engineering and Technology

All content in PEARL is protected by copyright law. Author manuscripts are made available in accordance with publisher policies. Please cite only the published version using the details provided on the item record or document. In the absence of an open licence (e.g. Creative Commons), permissions for further reuse of content should be sought from the publisher or author.

Title:

Performance of a plate-wave energy converter integrated in a floating breakwater

Journal:

IET Renewable Power Generation

Author names and affiliations:

S. Zheng[1;2]; M.H. Meylan[3]; X. Zhang[4]; G. Iglesias[5;2]; D. Greaves[2]

1 State Key Laboratory of Hydroscience and Engineering, Tsinghua University, Beijing, 100084, China
2 School of Engineering, Computing and Mathematics, University of Plymouth, Drake Circus, Plymouth PL4 8AA, UK
3 School of Mathematical and Physical Sciences, The University of Newcastle, Callaghan 2308, Australia
4 State Key Laboratory of Ocean Engineering, Shanghai Jiao Tong University, Shanghai, 200240, China
5 MaREI, Environmental Research Institute & School of Engineering, University College Cork, College Road, Cork, Ireland

Corresponding author

X. Zhang
E-mail: zhxt@sjtu.edu.cn

DOI: 10.1049/rpg2.12230

Submitted: February 27, 2021
Final revisions submitted: April 22, 2021
Accepted: May 11, 2021

IET Journals
The Institution of Engineering and Technology

Performance of a plate-wave energy converter integrated in a floating breakwater

ISSN 1751-8644
doi: 0000000000
www.ietdl.org

S. Zheng[1,2] *M.H. Meylan*[3] *X. Zhang*[4,*] *G. Iglesias*[5,2] *D. Greaves*[2]

[1] *State Key Laboratory of Hydroscience and Engineering, Tsinghua University, Beijing, 100084, China*
[2] *School of Engineering, Computing and Mathematics, University of Plymouth, Drake Circus, Plymouth PL4 8AA, UK*
[3] *School of Mathematical and Physical Sciences, The University of Newcastle, Callaghan 2308, Australia*
[4] *State Key Laboratory of Ocean Engineering, Shanghai Jiao Tong University, Shanghai, 200240, China*
[5] *MaREI, Environmental Research Institute & School of Engineering, University College Cork, College Road, Cork, Ireland*
* *E-mail: zhxt@sjtu.edu.cn*

Abstract: A plate-wave energy converter (pWEC) moored in front of a floating stationary breakwater is considered in this paper. The pWEC is composed of a submerged flexible plate with piezoelectric layers bonded to both faces of it. Hence the elastic motion of the plate excited by water waves can be transformed into useful electricity due to the piezoelectric effect. To evaluate the performance of the breakwater-attached pWEC in terms of wave power absorption and wave attenuation, a hydroelastic model based on linear potential flow theory and the eigenfunction matching method is developed with the electromechanical and the hydrodynamic problems of the pWEC coupled together. The pWEC can be either simply supported or clamped at the edge. A multi-parameter analysis is carried out with the employment of the present model. Effects of the width, submergence and edge types of the plate, together with the scales of the breakwater, including its width and draft, on wave power absorption and wave attenuation, are examined. As the pWEC moves towards a deeper position, the main peaks of the frequency response of the wave power absorption efficiency become lower and narrower. In contrast, its effect on wave attenuation is limited.

1 Introduction

Since the 1790s, many concepts for wave energy conversion have been proposed [1], the majority of which can be classified into five types: oscillating water column (OWC), overtopping device, point absorber, oscillating wave surge converter and raft-type device. Nevertheless, only a small range of wave energy converters have been tested at large scale and deployed in the sea [2]. The cost of power and survivability are two significant challenges that need to overcome to increase the commercial competitiveness of wave energy converters (WECs) in the global energy market.

To enhance the economics of the WECs and meanwhile improve their survivability, an effective way is to integrate them into coastal structures, such as breakwaters, jetties and piers or along sections of the coast, which would provide cost-sharing benefits, including construction, installation and maintenance [3, 4].

So far, most of the studies associated with integrating WECs into coastal structures have been focused on the OWC, overtopping and point absorber concepts.

Evans & Porter [5] studied the performance of an onshore OWC device composed of a thin vertical surface-piercing lip in front of a vertical wall. Their theoretical studies demonstrated that the incident wave power could be captured efficiently by choosing proper submergence of the lip and the spacing distance between the lip and the wall. To investigate the performance of OWCs installed along a straight coast/breakwater, Martins-Rivas & Mei [6] and Zheng et al. [7, 8] developed three-dimensional (3D) theoretical models and revealed that wave power extraction from the coast/breakwater integrated OWCs for a certain range of wave conditions can be significantly enhanced due to the constructive coast/breakwater reflection effect. He et al. [9] investigated the performance of a pile-supported OWC breakwater. They found that optimising power take-off damping for maximum power could lead to both satisfactory power extraction and wave transmission. Some other studies related to the integration of OWCs with coastal structures can be found in [10–16].

The hydrodynamic problem for the overtopping device is complicated. Most of the studies related to the integration of that device with coastal structures have been carried out using numerical simulation or/and physical model tests. An Overtopping BReakwater for Energy Conversion (OBREC) was designed to fully utilise traditional breakwaters and capturing wave energy [17]. Vicinanza et al. [17] carried out a series of physical tests of a 2-D OBREC model, discussed the wave loadings and average wave overtopping rate at its rear and front sides, and proposed a new design method for horizontal force on OBREC upper crown wall. Following their work [17], more recently, Contestabile et al. [18] completed the analysis on OBREC geometric parameter variation, with particular interest to the influence of the draft length, the reservoir width and the shape of the front ramp, and extended the overall knowledge on the device behaviour. The loading acting on the flat ramp was found to be greater than the curved ramp in almost all the tests by about 30–40%. Musa et al. [19] analysed the wave flow over the OBREC with the utilisation of FLOW 3D software and obtained a similar trend of the overtopping discharge when compared with the experimental data. Di Lauro et al. [20] performed numerical simulations based on the model IH2VOF, and studied the hydraulic performance and stability response of an OBREC device integrated into a vertical structure. The reflection coefficients of the OBREC were observed to be lower than those computed in front of the traditional breakwater. Comprehensive reviews associated with the OBREC can be found in [3, 21].

The integration of point absorbers into coastal structures has also been the object of recent work. Schay et al. [22] studied the hydrodynamic performance of a heaving point absorber near a fixed vertical wall in regular and irregular seas with a Boundary Element Method (BEM)-based software. Ning et al. [23] proposed an integrated system of a vertical pile-restrained floating breakwater working under the principle of a point absorber. The experimental test demonstrated that the system's capture width ratio was approximately 24%, whereas the transmission coefficient was lower than 0.50 with a proper power take-off damping force applied. More recently, Ning et al. [24], Zhao et al. [25] and Konispoliatis & Mavrakos [26] studied an array of point absorbers in front of a breakwater by using a BEM-based numerical code, physical testing and a theoretical model, respectively. Instead of focusing on the integration of point

© The Institution of Engineering and Technology 2015

absorbers into a conventional plane breakwater, Zhang & Ning [27] considered a novel breakwater with parabolic openings for wave energy harvesting. Their numerical studies showed that the reflected waves from the parabolic opening could travel towards a fixed focus position, stimulating wave power absorption of the point absorbers.

In addition to the five dominant types consisting of rigid bodies, there are some other WECs made from flexible structures, e.g., elastic plate [28] and bulge wave [29], which may offer improved performance/survivability and reduced cost compared with steel/concrete alternatives.

Zheng et al. [30, 31] proposed analytical models to study wave power absorption/dissipation of an array of floating/submerged porous elastic plates. Assuming the porosity of the elastic plates works as a simplified power take-off system, a profound potential of elastic plates was demonstrated for wave power extraction. The hydroelastics of a porous elastic plate in other circumstances, e.g., in two-layer fluids and in front of a vertical wall, was investigated by some other researchers [32, 33]. In fact, an elastic plate with piezoelectric layers bonded to both faces of the flexible substrate can extract energy from ocean waves [28]. Thanks to the piezoelectric effect, the tension variations at the plate-water interface of the plate WEC (pWEC) can be converted into a voltage, and the wave power is ultimately transformed into useful electricity. Renzi [28] developed a coupled hydro-electromechanical model, and evaluated the wave power absorption of a two dimensional (2D) submerged offshore stand-alone piezoelectric plate. Recently, this model was extended by Zheng et al. [34] to study the 3D hydroelastic problem of a circular stand-alone submerged piezoelectric pWEC. Buriani & Renzi [35] considered a submerged pWEC attached in front of a bottom-seated breakwater. It was demonstrated that the performance of the pWEC could be significantly improved due to the presence of the breakwater.

By contrast to the traditional bottom-seated breakwaters, floating breakwaters have less environmental impact since water and sediment are permitted to exchange between their seaside and leeside. Athanassoulis & Mamis [36] investigated a terminator-type piezoelectric system extracting electric energy from the direct impact of water waves impinging upon a vertical cliff, which could be formed by a floating breakwater. The wave power absorption of a cliff integrated piezoelectric system was reported to be as high as 30– 50% for appropriate hydro/piezo/electric parameters. Liu & Huang [37] considered the integration of piezoelectric material with a floating vertical flexible membrane breakwater and developed a theoretical model to study the performance of the system. It was revealed that the proposed system was suitable only at sites where the variability in the wave period is low due to the sensitivity of the transmission coefficient and the output power density on wave periods. In this paper, we consider a floating breakwater integrated piezoelectric pWEC. A 2D theoretical model is developed based on linear potential flow theory and the eigenfunction matching method to study the hydrodynamic performance of the system in terms of wave power absorption and wave attenuation. The proposed model is first validated by comparing the present results with published data and then applied to examine the effect of the width, submergence and edge conditions (i.e., simply supported and clamped) of the pWEC and the width and draft of the breakwater on wave power absorption and wave attenuation.

The rest of this paper is organised as follows: Section 2 outlines the mathematical model for the hydroelastic problem. Convergence analysis and validation of the present theoretical model are given in Sections 3 and 4, respectively. The validated model is then applied to carry out a multi-parameter study on the performance of the floating breakwater integrated pWEC in terms of wave power absorption and wave attenuation, the results of which can be found in Section 5. Finally, conclusions are drawn in Section 6.

2 Mathematical model

A pWEC moored in front of a floating stationary breakwater subjected to regular waves of amplitude A and angular frequency ω is considered (see Fig. 1). The waves propagate perpendicularly to the breakwater (i.e., wave crest-line is parallel with the breakwater). The pWEC is made from a flexible substrate with two piezoelectric layers bonded to both faces [28, 34]. The thicknesses of the substrate and the piezoelectric layers are much smaller compared with wavelength and water depth. Hence the pWEC may be assumed of negligible thickness in the hydrodynamic problem. The floating breakwater is assumed to be strictly constrained that its motion can be neglected, and it is considered stationary in the present work.

As shown in Fig. 1, Cartesian axes are chosen with the mean free–surface and front vertical wall of the breakwater coinciding with the planes of $z = 0$ and $x = 0$, respectively, x and z measured in the direction of wave propagation and vertically upwards, respectively. The length of the breakwater and the pWEC in the y-direction is assumed to be far longer than a wavelength so that the hydroelastic problem can be treated as a 2D one. The sea bed is at $z = -h$, and the pWEC with a width l is placed at $z = -d$. The width and draft of the breakwater are denoted by l_0 and d_0, respectively. The fluid domain is divided into five regions (Fig. 1b), which we will use in the solution process, i.e., Ω_1, the seaside outer region ($x \in (-\infty, -l]$, $z \in [-h, 0]$); Ω_{2a}, the region above the pWEC ($x \in [-l, 0]$, $z \in [-d, 0]$); Ω_{2b}, the region below the pWEC ($x \in [-l, 0]$, $z \in [-h, -d]$); Ω_3, the region under the floating breakwater ($x \in [0, l_0)$, $z \in [-h, -d_0]$) and Ω_4, the leeside outer region ($x \in [l_0, \infty)$, $z \in [-h, 0]$).

2.1 Problem formulation

All amplitudes are assumed to be small enough that linear theory applies, and the fluid is assumed to be inviscid, incompressible and irrotational. It is further assumed that all motion is time-harmonic with the angular frequency ω; hence the fluid velocity potential and the displacement of the plate about $z = -d$ may be expressed by

$$\Phi(x, z, t) = \mathrm{Re}\{\phi(x, z)\mathrm{e}^{-\mathrm{i}\omega t}\}, \tag{1}$$

and

$$\tilde{\xi}(x, t) = \mathrm{Re}\{\xi(x)\mathrm{e}^{-\mathrm{i}\omega t}\}, \tag{2}$$

where Re denotes the real part. The functions $\phi(x, z)$ and $\xi(x)$ represent the time-independent parts of the complex velocity potential and the plate displacement, respectively.

Under the assumptions above, the spatial velocity potential satisfies the Laplace equation in the fluid with the boundary conditions

$$\partial_z\phi = \frac{\omega^2}{g}\phi \ \text{ on } \ z = 0, \ x \in (-\infty, 0] \cup [l_0, \infty) \tag{3}$$

$$\partial_z\phi = 0 \quad \text{on } \ z = -h \tag{4}$$

$$\partial_z\phi = 0 \quad \text{on } \ z = -d_0, \ x \in [0, l_0] \tag{5}$$

$$\partial_x\phi = 0 \quad \text{on } \ x = 0 \text{ and } l_0, \ z \in [-d_0, 0] \tag{6}$$

$$\partial_z\phi\Big|_{z=-d_+} = \partial_z\phi\Big|_{z=-d_-} \quad \text{on } \ x \in [-l, 0] \tag{7}$$

where $+$ and $-$ denote above and below the plate, respectively. The scattered wave field consists of outgoing waves only with a finite value at $|x| = \infty$.

Additionally, the time-independent spatial velocity potential, ϕ, at the interface of the regions Ω_{2a} and Ω_{2b} should be coupled to the plate displacement function, ξ, in terms of both kinematic and

© The Institution of Engineering and Technology 2015

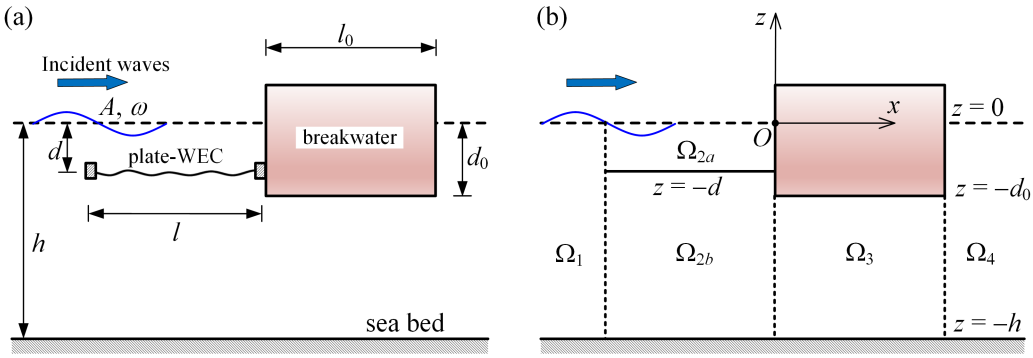

Fig. 1: Schematic diagram of a floating breakwater integrated pWEC: (a) side view in physical variables; (b) fluid domain decomposition used in the mathematical model.

dynamic conditions [28],

$$\partial_z\phi = -\mathrm{i}\omega\xi \ \text{ on } \ x \in [-l, 0]\,, z = -d, \tag{8}$$

$$g\chi\left(1 + \frac{\beta^2\zeta\omega}{\mathrm{i}+\zeta\omega}\right)\partial_x^4\xi - \omega^2\gamma\xi = \mathrm{i}\omega(\phi_- - \phi_+) \quad \text{on } \ x \in [-l, 0]\,, z = -d, \tag{9}$$

in which $+$ and $-$ denote above and below the plate, respectively;

$$\chi = \frac{B'}{\rho g}, \ \ \beta = \frac{\theta'}{\sqrt{B'C'}}, \ \ \zeta = \frac{C'}{G'}, \ \ \gamma = \frac{I_b'}{\rho}, \tag{10}$$

where B' represents the flexural rigidity of the bimorph, θ' is a piezoelectric coupling factor, C' denotes the electrical surface capacitance, G' is the surface conductance, I_b' represents the surface density of the bimorph, $I_b' = \rho_0 d_0 + 2\rho_\mathrm{p} d_\mathrm{p}$, in which ρ_0 and ρ_p denote the densities of the substrate and the piezoelectric layers, respectively. d_0 and d_p represent the thicknesses of the substrate and the piezoelectric layers, respectively. ρ is the fluid density. In this paper, the bimorph piezoelectric plate is characterised by d_0 = 0.01 m, $d_\mathrm{p} = 1.1 \times 10^{-4}$ m, $\rho_0 = 1250\,\mathrm{kg/m^3}$, $\rho_\mathrm{p} = 1780\,\mathrm{kg/m^3}$ (for details see [38] and [28]).

The two components as given above can be combined into

$$\left[\chi\left(1 + \frac{\beta^2\zeta\omega}{\mathrm{i}+\zeta\omega}\right)\partial_x^4 - \frac{\omega^2}{g}\gamma\right]\partial_z\phi + \frac{\omega^2}{g}(\phi_+ - \phi_-) = 0 \quad \text{on } x \in [-l, 0]\,, z = -d, \tag{11}$$

which couples the electro-mechanical and the hydrodynamic problems at the plate-water interface.

We also need to apply edge conditions at the plate end. If the plate is simply supported, the edge conditions are

$$\xi(0) = \partial_x^2\xi(0) = \xi(-l) = \partial_x^2\xi(-l) = 0 \tag{12}$$

and they read

$$\xi(0) = \partial_x\xi(0) = \xi(-l) = \partial_x\xi(-l) = 0 \tag{13}$$

for a plate whose edge is clamped.

2.2 *Expressions of the velocity potentials in different regions*

2.2.1 Regions Ω_1 and Ω_4: The eigenfunction expansion in these regions is completely standard and follows from [39, 40], and we only summarise the results here.

Region Ω_1 $\{x \in (-\infty, -l], z \in [-h, 0]\}$

Expression of the spatial velocity potential in Region Ω_1 may be written as

$$\phi_1 = -\frac{\mathrm{i}gA}{\omega}\mathrm{e}^{\mathrm{i}kx}Z_0(z) + \sum_{n=0}^{\infty} A_n\mathrm{e}^{-\mathrm{i}k_n x}Z_n(z), \tag{14}$$

where the first term on its right-hand side represents the undisturbed incident spatial velocity potential, ϕ_I. A_n are the unknown coefficients to be determined. $k_0 = k \in \mathbb{R}^+$ and $k_n \in \mathrm{i}\mathbb{R}^+$ for $n = 1, 2, \cdots$ support the propagating waves and evanescent waves, respectively, and they are the positive real root and the infinite positive imaginary roots of the dispersion equation,

$$\frac{\omega^2}{g} = k_n\tanh(k_n h); \tag{15}$$

The corresponding depth functions $Z_n(z)$ are expressed as

$$Z_n(z) = \frac{\cosh[k_n(z+h)]}{\cosh(k_n h)}. \tag{16}$$

Region Ω_4 $\{x \in [l_0, \infty), z \in [-h, 0]\}$

Expression of the spatial velocity potential in Region Ω_4 can be expressed as

$$\phi_4 = \sum_{n=0}^{\infty} B_n\mathrm{e}^{\mathrm{i}k_n x}Z_n(z), \tag{17}$$

where B_n are the unknown coefficients to be determined.

2.2.2 Region Ω_2 $\{z \in [-h, 0], x \in [-l, 0]\}$: In region Ω_2, the potential may be written as

$$\phi_2(x, z) = \sum_{n=-2}^{\infty}(C_n\mathrm{e}^{\kappa_n x} + D_n\mathrm{e}^{-\kappa_n x})Y_n(z), \tag{18}$$

where C_n and D_n are the unknown coefficients to be determined;

$$Y_n(z) = \begin{cases} -\sin(\kappa_n c)\left[\kappa_n h\cos(\kappa_n z) + \dfrac{\omega^2}{g}h\sin(\kappa_n z)\right], \\ \qquad\qquad \text{on } \ z \in [-d, 0) \\ \cos[\kappa_n(z+h)]\left[\kappa_n h\sin(\kappa_n d) + \dfrac{\omega^2}{g}h\cos(\kappa_n d)\right], \\ \qquad\qquad \text{on } \ z \in [-h, -d] \end{cases} \tag{19}$$

in which $c = h - d$; κ_n for $n = -2, -1, 0, 1, 2, \cdots$ are the roots of the dispersion relation for the pWEC,

$$\left[\chi\left(1 + \frac{\beta^2\zeta\omega}{\mathrm{i}+\zeta\omega}\right)\kappa^4 - \frac{\omega^2}{g}\gamma\right]\left[\kappa\sin(\kappa d) + \frac{\omega^2}{g}\cos(\kappa d)\right]\tan(\kappa c) = -\frac{\omega^2}{g}\left\{\left[\cos(\kappa d) - \frac{\omega^2}{g\kappa}\sin(\kappa d)\right]\tan(\kappa c) + \sin(\kappa d) + \frac{\omega^2}{g\kappa}\cos(\kappa d)\right\}, \tag{20}$$

© The Institution of Engineering and Technology 2015

which can be derived by inserting Eq. (18) into Eq. (11).

Particularly, if $\beta = 0$ or $\zeta = 0$, the plate turns into a submerged elastic plate, for which the corresponding properties of the roots can be found in [41]. Once the roots for $\beta = 0$ or $\zeta = 0$ are determined, the roots of the dispersion relation for $\beta \neq 0$ and $\zeta \neq 0$ can then be derived by using the homotopy method, starting with the corresponding roots for the case of $\beta = 0$ or $\zeta = 0$ [42, 43].

2.2.3 Region Ω_3 $\{x \in [0, l_0],\ z \in [-h, -d_0]\}$: The velocity potential in the fluid domain under the breakwater, i.e., Region Ω_3 can be expressed as

$$\phi_3(x,z) = E_0 x + F_0 + \sum_{n=1}^{\infty}(E_n \mathrm{e}^{\beta_n x} + F_n \mathrm{e}^{-\beta_n x})\cos[\beta_n(z+h)], \tag{21}$$

where $\beta_n = \frac{n\pi}{h-d_0}$; E_n and F_n for $n = 0,\ 1,\ 2,\ \cdots$ are the unknown coefficients to be determined.

2.3 Continuity conditions

Continuity conditions at the interfaces of the adjacent regions and the side wall of the breakwater should be satisfied:

$$\phi_1|_{x=-l} = \phi_2|_{x=-l}, \quad z \in [-h, 0] \tag{22}$$

$$\phi_2|_{x=0} = \phi_3|_{x=0}, \quad z \in [-h, -d_0] \tag{23}$$

$$\phi_3|_{x=l_0} = \phi_4|_{x=l_0}, \quad z \in [-h, -d_0] \tag{24}$$

$$\partial_x\phi_1|_{x=-l} = \partial_x\phi_2|_{x=-l}, \quad z \in [-h, 0], \tag{25}$$

$$\partial_x\phi_2|_{x=0} = \begin{cases} 0, & z \in [-d_0, 0], \\ \partial_x\phi_3|_{x=0}, & z \in [-h, -d_0], \end{cases} \tag{26}$$

$$\partial_x\phi_4|_{x=l_0} = \begin{cases} 0, & z \in [-d_0, 0], \\ \partial_x\phi_3|_{x=l_0}, & z \in [-h, -d_0]. \end{cases} \tag{27}$$

These continuity conditions, together with the edge conditions, can form a linear algebraic system after truncation of the infinite series of vertical eigenfunctions at N, and can be further employed to determine the unknown coefficients A_n, B_n, C_n, D_n, E_n and F_n. The complicated deduction process of the formulas and calculation of these unknown coefficients are given in the Appendix, i.e., Section 8.

2.4 Free-surface elevation

The elevation of the air–water interface vertically deviating from the still water level, i.e., the free-surface elevation, is expressed as:

$$\eta_0(x) = \frac{\mathrm{i}\omega}{g}\phi|_{z=0}. \tag{28}$$

2.5 Plate displacement

The displacement of the pWEC about $z = -d$ can be calculated in terms of C_n and D_n as

$$\xi = \frac{\mathrm{i}}{\omega}\partial_z\phi|_{z=-d} = -\frac{\mathrm{i}}{\omega}\sum_{n=-2}^{\infty}\kappa_n \sin(\kappa_n c)\big[\kappa_n h \sin(\kappa_n d) + \frac{\omega^2}{g}h\cos(\kappa_n d)\big](C_n \mathrm{e}^{\kappa_n x} + D_n \mathrm{e}^{-\kappa_n x}). \tag{29}$$

2.6 Hydrodynamic force acting on the plate

The vertical hydrodynamic force acting on the plate can be calculated by integrating the hydrodynamic pressure drop across the pWEC over $x \in [-l, 0]$

$$\begin{aligned} F_e &= \mathrm{i}\omega\rho\int_{-l}^{0}(\phi_- - \phi_+)|_{z=-d}\mathrm{d}x \\ &= \mathrm{i}\omega\rho\sum_{n=-2}^{\infty}[C_n(1-\mathrm{e}^{-\kappa_n l}) - D_n(1-\mathrm{e}^{\kappa_n l})] \\ &\times\left(h\sin(\kappa_n h) + \frac{\omega^2 h}{g\kappa_n}\cos(\kappa_n h)\right). \end{aligned} \tag{30}$$

2.7 Wave reflection and transmission

The wave reflection and transmission coefficients denoted by R and T, respectively, can be calculated by

$$R = \frac{\omega}{gA}|A_0|, \quad T = \frac{\omega}{gA}|B_0|. \tag{31}$$

2.8 Wave power absorption

2.8.1 Direct method: Wave power absorption by the pWEC may be evaluated in a straightforward manner following [28, 35]

$$\begin{aligned} P_{\mathrm{ext}} &= \frac{\omega^2\rho g}{2}\frac{\beta^2\chi\zeta}{1+\omega^2\zeta^2}\int_{-l}^{0}|\partial_x^2\xi|^2\mathrm{d}x \\ &= \frac{\rho g}{2}\frac{\beta^2\chi\zeta}{1+\omega^2\zeta^2}\int_{-l}^{0}|\partial_z^3\phi|_{z=-d}|^2\mathrm{d}x, \\ &= \frac{\rho g}{2}\frac{\beta^2\chi\zeta}{1+\omega^2\zeta^2}\Bigg\{\sum_{n=-2}^{\infty}\sum_{m=-2}^{\infty}\kappa_n^3\kappa_m^{*3}\sin(\kappa_n c)\sin(\kappa_m^* c) \\ &\times\big[\kappa_n h\sin(\kappa_n d) + \frac{\omega^2}{g}h\cos(\kappa_n d)\big] \\ &\times\big[\kappa_m^* h\sin(\kappa_m^* d) + \frac{\omega^2}{g}h\cos(\kappa_m^* d)\big] \\ &\times\Big[\frac{C_n C_m^*(1-\mathrm{e}^{-(\kappa_n+\kappa_m^*)l})}{\kappa_n+\kappa_m^*} - \frac{D_n D_m^*(1-\mathrm{e}^{(\kappa_n+\kappa_m^*)l})}{\kappa_n+\kappa_m^*} \\ &+\frac{C_n D_m^*(1-\mathrm{e}^{-(\kappa_n-\kappa_m^*)l})}{\kappa_n-\kappa_m^*} - \frac{C_m^* D_n(1-\mathrm{e}^{(\kappa_n-\kappa_m^*)l})}{\kappa_n-\kappa_m^*}\Big]\Bigg\} \end{aligned} \tag{32}$$

We introduce the relative absorbed power, i.e., wave power absorption efficiency

$$\eta_{ext} = \frac{P_{ext}}{P_{inc}}, \tag{33}$$

where

$$P_{inc} = \frac{\rho g A^2}{2}\frac{\omega}{2k}\left(1 + \frac{2kh}{\sinh(2kh)}\right) \tag{34}$$

denotes the incoming wave power.

2.8.2 Indirect method: Apart from the direct method, an indirect method can be derived based on Green's theorem

$$\begin{aligned} P_{ext} = \frac{\rho\omega}{4\mathrm{i}}\int_{-h}^{0}\Bigg[&\left(\phi\frac{\partial\phi^*}{\partial x} - \phi^*\frac{\partial\phi}{\partial x}\right)\Bigg|_{x=X} \\ &-\left(\phi\frac{\partial\phi^*}{\partial x} - \phi^*\frac{\partial\phi}{\partial x}\right)\Bigg|_{x=-X}\Bigg]\mathrm{d}z, \end{aligned} \tag{35}$$

where $X > \max\{l, l_0\}$. When $X \to \infty$, only propagating waves remain, and Eq. (35) can be rewritten as

$$P_{ext} = \frac{\rho\omega[\sinh(kh)\cosh(kh) + kh]}{4\cosh^2(kh)}\left(\frac{g^2A^2}{\omega^2} - |A_0|^2 - |B_0|^2\right), \tag{36}$$

© The Institution of Engineering and Technology 2015

resulting in the corresponding wave power absorption efficiency

$$\eta_{ext} = 1 - R^2 - T^2, \tag{37}$$

which is in line with the energy conservation, indicating the incident wave power is absorbed, reflected and transmitted by the breakwater integrated pWEC.

3 Convergence analysis

Figure 2 illustrates the impact of the truncated cutoffs (i.e., in terms of N) on the frequency response of wave power absorption efficiency and wave transmission coefficient for a floating breakwater integrated pWEC with $l_0/h = 0.5$, $d_0/h = 0.5$, $l/h = 1.0$, $d/h = 0.2$, $\bar{\chi} = \chi/h^4 = 4.78 \times 10^{-7}$, $\bar{\gamma} = \gamma/h = 1.258 \times 10^{-3}$, $\beta = 0.24$ and $\bar{\zeta} = \zeta\sqrt{g/h} = 1.0$. In order to obtain the converged results, $N \geq 40$ is suggested. Hereinafter, $N = 40$ is adopted.

4 Model validation

When $d_0/h = 1.0$ (or $d_0/h \to 1.0$), the bottom of the floating breakwater touches (or approaches) the sea bed, making the system become (or work similar to) a pWEC mooring in front of a bottom-seated breakwater, the hydrodynamic problem of which has already been numerically studied by Buriani & Renzi [35]. Moreover, if either χ or γ is large enough, the pWEC would work as a rigid plate, and the present hydrodynamic problem becomes the wave reflection by a vertical wall with a horizontal submerged rigid plate studied by Wu et al. [44]. Figure 3 presents a comparison of wave power absorption efficiency between the present results and those of [35]. Variation of the free-surface elevation at $x = 0$ and the vertical hydrodynamic force acting on the pWEC for $\bar{\chi} = \chi/h^4 = 10^4$ versus pWEC width, together with the corresponding published data associated with a rigid plate placed in front of a vertical wall [44], are plotted in Fig. 4.

If the width of the pWEC is small enough, the floating breakwater integrated pWEC is expected to work as a single breakwater. Figure 5 illustrates the comparison of the wave reflection/transmission coefficients of a floating breakwater integrated pWEC with $l_0/h = 0.5$, $d_0/h = 0.5$, $l/h = 0.01$, $d/h = 0.2$, and those of a single isolated breakwater [39].

In addition to the above three extreme circumstances, a more general case with $l_0/h = 0.5$, $d_0/h = 0.5$, $l/h = 1.0$, $d/h = 0.2$ is examined, the wave power absorption efficiency of which is calculated by using both the direct and indirect methods, and the comparison between them is illustrated in Fig. 6.

The excellent agreement between the results shown in Figs. 3, 4, 5 and 6 gives confidence in the present model for solving the problem of wave interaction with a floating breakwater integrated pWEC.

5 Results and discussion

In this section, the validated model is adapted to study the effects of the pWEC width, pWEC submergence, breakwater width and breakwater draft, together with the type of the pWEC edge, on wave power absorption and wave attenuation of the floating breakwater integrated pWEC.

5.1 Effect of the plate edge type

Fig. 7 shows that the performance of the pWEC in terms of wave power absorption is dramatically influenced by the edge types. In the computed range of wave frequencies, i.e., $\omega^2 h/g \in [0.1, 2.5]$, there are three and four peaks of the $\eta_{ext} - \omega^2 h/g$ curves observed for the clamped and simply supported edge conditions, respectively. For the clamped edge condition, the peak values of η_{ext} and the corresponding $\omega^2 h/g$ are $(0.22, 0.29)$, $(0.07, 0.71)$ and $(0.58, 1.51)$. Correspondingly, for the simply supported edge conditions, they are $(0.06, 0.20)$, $(0.01, 0.51)$, $(0.28, 1.14)$ and $(0.57, 2.26)$.

This may be explained from the point of view of resonance. The more strictly the plate edge is constrained, the larger the stiffness of the plate, resulting in larger wave frequencies where the peaks occur.

The transmission coefficient presents an overall decreasing trend with increase of the wave frequency (Fig. 7b). Several sudden drops of T are observed at the frequencies where the peaks of η_{ext} happen.

Figure 8 presents a snapshot of the system with the displacements of the pWEC and the free-surface elevation at the seaside and leeside of the breakwater. The incident water waves have amplitude A= 0.2 m and period of 5 s, corresponding to a wavelength of 36.58 m. The free surface is found to match seamlessly across Regions Ω_1 and Ω_{2a} defined in subsection 2.2 (Fig. 1b). The clamping (i.e., Eq. (13)) and simply supported (i.e., Eq. (12)) edge conditions are correctly satisfied by the analytical solutions. On the plate, short-crested oscillations are created by a short, weakly damped progressive wave, which has also been reported by Renzi [28] for an offshore stand-alone pWEC. This can be explained from the properties of the root of the dispersion equation for the pWEC. Due to the coupled hydroelectromechanical effect, a coupled system of long- and short-crested weakly damped flexural waves with the length of 36.56 m and 2.72 m, which correspond to the roots $\kappa_0 = (-7.73 \times 10^{-9} + 1.72 \times 10^{-1}\mathrm{i})\ \mathrm{m}^{-1}$ and $\kappa_1 = (-1.25 \times 10^{-2} + 2.31\mathrm{i})\ \mathrm{m}^{-1}$, respectively, are excited by the incident waves. For the present case, the short-crested weakly damped flexural wave dominates the plate displacements.

5.2 Effect of the plate width, l

Figure 9 plots the wave power absorption efficiency and wave transmission coefficient of the floating breakwater integrated pWEC against $\omega^2 h/g$ for different values of pWEC width in terms of l/h. In the computed range of wave frequencies, the larger the width of the pWEC, the more peaks of the $\eta_{ext} - \omega^2 h/g$ are observed. This can be explained from the view of the natural vibration frequencies of a beam with fixed ends and distributed mass, which are proportional to l^{-2}.

For most of the cases studied, the larger the wave frequencies where the peaks of the $\eta_{ext} - \omega^2 h/g$ occur, the larger the peaks in terms of both the peak value and bandwidth are observed. It is noted that $\eta_{ext} > 0.8$ can be achieved at specified wave frequencies for the cases with $l/h = 0.7$, 1.3 and 1.6.

Unlike the wave power absorption efficiency (Fig. 9a), the wave transmission coefficients plotted in Fig. 9b are found to be rather insensitive to the change of pWEC width, unless the peaks of η_{ext} occur, making the $T - \omega^2 h/g$ curves present a local inverted 'N' shape.

The integrated system has a dual-function of wave power absorption and wave attenuation. The effective frequency bandwidth simultaneously satisfied with the requested absorption efficiency and transmission coefficient may be of interest. In the computed range of wave frequencies, the nondimensional frequency bandwidths with $\eta_{ext} > 0.3$ and $T < 0.3$ are 0.01 ([2.49, 2.50]), 0.20 ([1.71, 1.91]), 0.07 ([1.47, 1.53]), 0.27 ([2.17, 2.44]) and 0.20 ([1.88, 2.09]) for $l/h = 0.4$, 0.7, 1.0, 1.3 and 1.6, respectively. Hence, from the perspective of the effective dual-function, the $l/h = 1.3$ case may be the most promising among the five cases examined.

5.3 Effect of the plate submergence, d

The submergence of the plate is one of the key parameters affecting the roots of the dispersion equation for the pWEC (see Eq. (20)), and is expected to influence the hydroelastics of the pWEC further. The system with $d/h = 0.1$, 0.15, 0.2, 0.25 and 0.3 are selected as fives cases to examine the effect of the pWEC submergence on wave power absorption and wave attenuation (Fig. 10).

As indicated in Fig. 10a, as d/h increases, the main peaks of η_{ext} around $\omega^2 h/g = 1.5$ become lower and narrower. This could be because most wave power is concentrated at less than one-quarter of a wavelength below the water level, and the kinetic energy at a deeper position is less intensive than that at a shallower position. However, it should be noted that the other two peaks located at

© The Institution of Engineering and Technology 2015

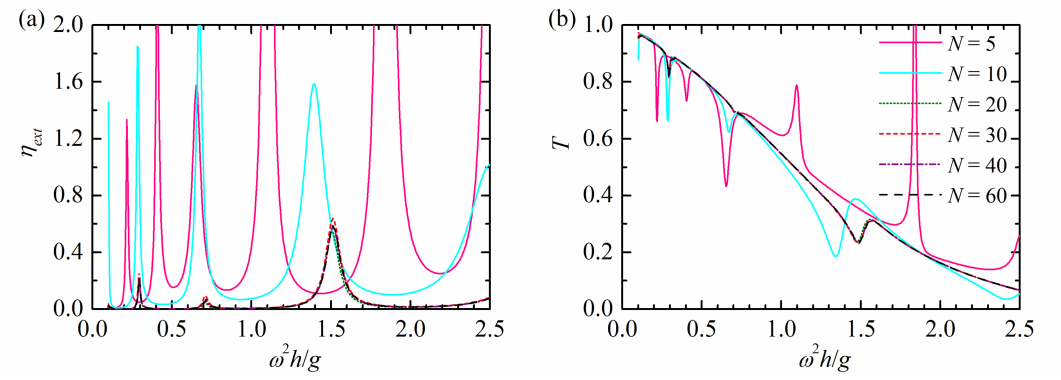

Fig. 2: Impact of the truncated cut-offs (i.e., in terms of N) on wave power absorption and wave attenuation, $l_0/h = 0.5$, $d_0/h = 0.5$, $l/h = 1.0$, $d/h = 0.2$, $\bar{\chi} = \chi/h^4 = 4.78 \times 10^{-7}$, $\bar{\gamma} = \gamma/h = 1.258 \times 10^{-3}$, $\beta = 0.24$ and $\bar{\zeta} = \zeta\sqrt{g/h} = 1.0$: (a) η_{ext}; (b) T.

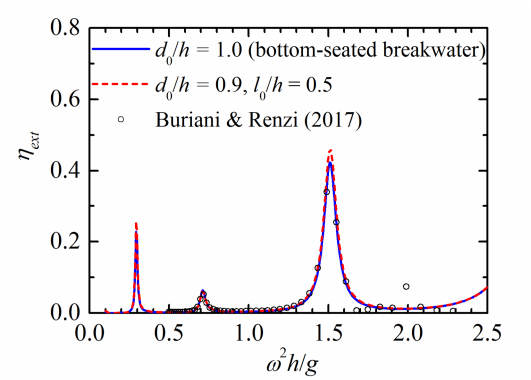

Fig. 3: Frequency response of wave power absorption efficiency, $l/h = 1.0$, $d/h = 0.2$, $\bar{\chi} = \chi/h^4 = 4.78 \times 10^{-7}$, $\bar{\gamma} = \gamma/h = 1.258 \times 10^{-3}$, $\beta = 0.24$ and $\bar{\zeta} = \zeta\sqrt{g/h} = 1.0$.

$\omega^2 h/g \approx 0.3$ and 0.7 (corresponding to the wavelength of 108.96 m and 66.31 m, respectively) become higher with the increase of d/h. For these wave conditions, the wavelength is long enough that the kinetic energy is almost independent of the vertical position in the fluid domain, and does not dominate wave power absorption of the pWEC any more.

With the increase of d/h, the peaks of η_{ext} shift towards high wave frequencies, and this may be explained from the view of added-mass, which increases as d/h becomes larger [45], resulting in larger natural resonant frequencies.

The wave transmission coefficient as plotted in Fig. 10b is found to be insensitive to the change of the pWEC submergence.

5.4 *Effect of the breakwater width, l_0*

The effect of the breakwater width on wave power absorption and wave attenuation is illustrated in Fig. 11. As expected, the $T - \omega^2 h/g$ curves descend along with the raise of breakwater width (Fig. 11b). It is also expected that when the breakwater is wide enough, it will work like a bottom-seated breakwater and that no wave power will be transmitted to its leeside.

In contrast to the change of the breakwater width on wave attenuation, its influence on wave power absorption of the pWEC is found to be rather limited (Fig. 11a). As l_0/h increases from 0.1 to 0.9, the peak value of η_{ext} around $\omega^2 h/g = 1.5$ decreases merely by 11.6% from 0.62 to 0.55. It should be emphasised that this is a 'decrease' change of η_{ext}, although not too much, instead of 'increase', meaning that enlarging the breakwater width not only weakens wave attenuation but also suppresses wave power absorption of the pWEC.

5.5 *Effect of the breakwater draft, d_0*

The effect of varying the breakwater draft on wave absorption and wave attenuation is also investigated by examining five cases with d_0/h ranging from 0.3 to 0.7 with a step of 0.1 (Fig. 12).

As demonstrated in Fig. 12, the variation of d_0/h plays a similar role as that of the breakwater width l_0/h on the performance of the floating breakwater integrated pWEC as plotted in Fig. 11, but in a more dramatic manner. More specifically, as d_0/h increases from 0.3 to 0.7, the main peak value of η_{ext} drops from 0.66 to 0.52 by 21.7%. Moreover, the bandwidth of the main peak is compressed.

For $d_0/h = 1.0$, $\partial_x \phi = 0$, i.e., null horizontal fluid velocity, should be satisfied at $x = 0$ all over the water depth, i.e., the fluid particles below the pWEC are not allowed to pass through the plane of $x = 0$. As a comparison, for $d_0/h < 1.0$, the fluid particles under the pWEC are free to move across $x = 0$ for $z \in [-h, -d_0]$, which may further liberate the motion of the pWEC and ultimately enhance wave power absorption.

6 Conclusions

In this paper, a pWEC moored in front of a floating breakwater is considered. The pWEC consists of a submerged flexible plate with piezoelectric layers bonded to both faces of it. The elastic motion of the plate can be transformed into useful electricity due to the piezoelectric effect. To evaluate the performance of the system, a 2D theoretical model is proposed based on linear potential flow theory and the eigenfunction matching method coupling the electromechanical and the hydrodynamic problems.

The theoretical model was first validated by comparing the present results with published data for different extreme cases, and an excellent agreement between them was achieved. The validated model was ultimately applied to explore the influence of the edge condition, width and submergence of the pWEC and the width and draft of the breakwater on wave power absorption and wave attenuation. The following conclusions may be drawn:

1. Wave power absorption of the pWEC is dramatically influenced by the edge types. There are three and four peaks of the $\eta_{ext} - \omega^2 h/g$ curves in the computed range of wave frequencies for the clamped and simply supported edge conditions, respectively.

2. As the width of the pWEC increases, more peaks of the $\eta_{ext} - \omega^2 h/g$ curves can be excited. As pWEC moves towards a deeper position, the main peaks of η_{ext} around $\omega^2 h/g = 1.5$ become lower and narrower. Varying the width or submergence of the pWEC, the influence on wave attenuation of the system is limited.

3. Wave transmission coefficient can be effectively reduced all over the examined wave frequencies by increasing either the width or the draft of the breakwater. Nevertheless, the change of the breakwater

© The Institution of Engineering and Technology 2015

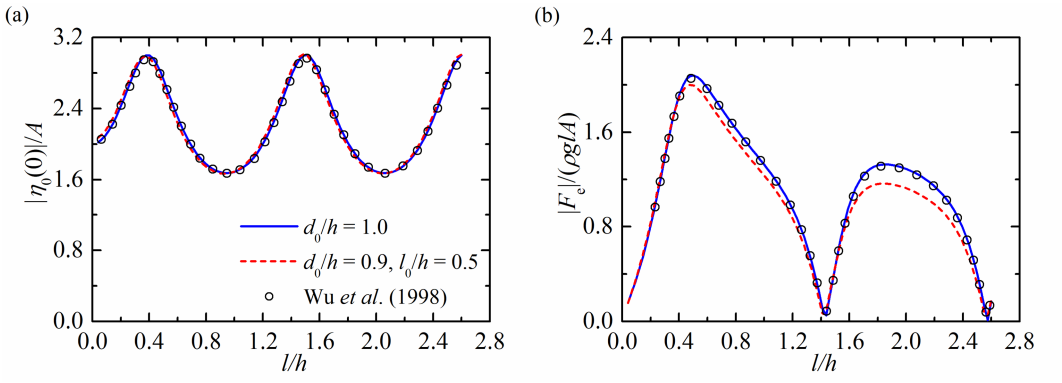

Fig. 4: Variation of wave amplitude at $x = 0$ and the hydrodynamic wave force acting on the plate versus plate length, $\omega^2 h/g = 1.44$ (wavelength = $4.0h$), $d/h = 0.2$, $\bar{\chi} = \chi/h^4 = 10^4$, $\bar{\gamma} = \gamma/h = 1.258 \times 10^{-3}$, $\beta = 0.24$ and $\bar{\zeta} = \zeta\sqrt{g/h} = 1.0$: (a) $|\eta_0|/A$; (b) $|F_e|/\rho g l A$.

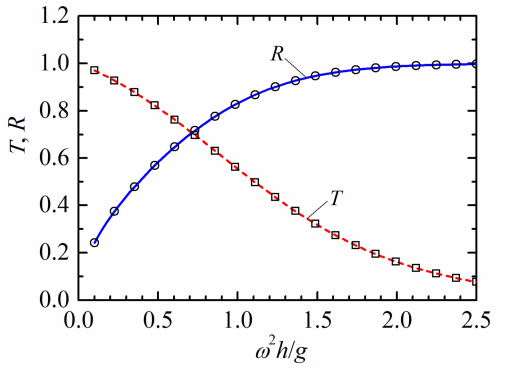

Fig. 5: Frequency response of the wave transmission coefficient and reflection coefficient, $l_0/h = 0.5$, $d_0/h = 0.5$, Lines: present results with $l/h = 0.01$, $d/h = 0.2$, $\bar{\chi} = \chi/h^4 = 4.78 \times 10^{-7}$, $\bar{\gamma} = \gamma/h = 1.258 \times 10^{-3}$, $\beta = 0.24$ and $\bar{\zeta} = \zeta\sqrt{g/h} = 1.0$; Symbols: Zheng & Zhang [39].

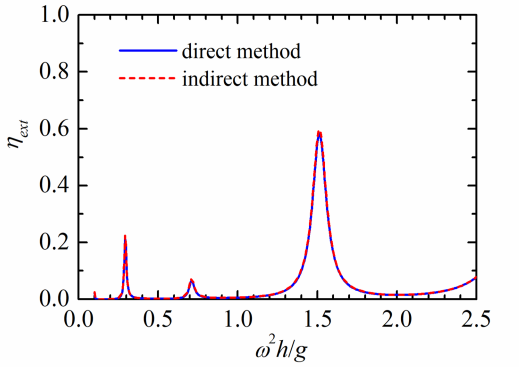

Fig. 6: Frequency response of the wave power absorption efficiency, $l_0/h = 0.5$, $d_0/h = 0.5$, $l/h = 1.0$, $d/h = 0.2$, $\bar{\chi} = \chi/h^4 = 4.78 \times 10^{-7}$, $\bar{\gamma} = \gamma/h = 1.258 \times 10^{-3}$, $\beta = 0.24$ and $\bar{\zeta} = \zeta\sqrt{g/h} = 1.0$.

width/draft has limited influence on wave power absorption of the pWEC.

The present work is focused on the hydroelastic problem of a breakwater integrated pWEC with a fixed distributed–parameter model of the piezoelectric system adopted from [28, 35]. The device's wave power absorption could be enhanced if the piezoelectric system can be appropriately selected and optimised. The breakwater was assumed to be stationary, and its oscillation was not registered in our present model. However, this is an aspect of interest that we plan to investigate as a continuation of this line of research. How to broaden the effective frequency bandwidth for such an integrated system is also an interesting research topic for future work.

Acknowledgements

The research was supported by Open Research Fund Program of State key Laboratory of Hydroscience and Engineering (Tsinghua University) (grant no. sklhse-2021-E-02) and Open Research Fund Program of State Key Laboratory of Ocean Engineering (Shanghai Jiao Tong University) (grant no. 1916). S.Z. was supported by the European Union funded Marine-I (2nd phase) project (grant no. 05R18P02816). S.Z. wishes to thank Prof. Bin Teng from Dalian University of Technology for valuable discussions. X.Z. was supported by the 2020 Research Program of Sanya Yazhou Bay Science and Technology City (grant no. SKJC-2020-01-006) and Hainan Provincial Natural Science Foundation of China (grant no. 520QN290)

7 References

1 Clément, A., McCullen, P., Falcão, A.F.d.O., Fiorentino, A., Gardner, F., Hammarlund, K., et al.: 'Wave energy in Europe: current status and perspectives', *Renewable and Sustainable Energy Reviews*, 2002, **6**, (5), pp. 405–431
2 Drew, B., Plummer, A.R., Sahinkaya, M.N.: 'A review of wave energy converter technology', *Proceedings of the Institution of Mechanical Engineers Part A-Journal of Power and Energy*, 2009, **223**, (A8), pp. 887–902
3 Mustapa, M.A., Yaakob, O.B., Ahmed, Y.M., Rheem, C.K., Koh, K.K., Adnan, F.A.: 'Wave energy device and breakwater integration: A review', *Renewable and Sustainable Energy Reviews*, 2017, **77**, pp. 43–58
4 Zhang, H., Zhou, B., Vogel, C., Willden, R., Zang, J., Zhang, L.: 'Hydrodynamic performance of a floating breakwater as an oscillating-buoy type wave energy converter', *Applied Energy*, 2020, **257**, pp. 113996
5 Evans, D.V., Porter, R.: 'Hydrodynamic characteristics of an oscillating water column device', *Applied Ocean Research*, 1995, **17**, (3), pp. 155–164
6 Martins.rivas, H., Mei, C.C.: 'Wave power extraction from an oscillating water column along a straight coast', *Ocean Engineering*, 2009, **36**, (6-7), pp. 426–433
7 Zheng, S., Zhang, Y., Iglesias, G.: 'Coast/breakwater-integrated OWC: A theoretical model', *Marine Structures*, 2019, **66**, pp. 121 – 135
8 Zheng, S., Antonini, A., Zhang, Y., Greaves, D., Miles, J., Iglesias, G.: 'Wave power extraction from multiple oscillating water columns along a straight coast', *Journal of Fluid Mechanics*, 2019, **878**, pp. 445–480
9 He, F., Zhang, H., Zhao, J., Zheng, S., Iglesias, G.: 'Hydrodynamic performance of a pile-supported OWC breakwater: An analytical study', *Applied Ocean Research*, 2019, **88**, pp. 326 – 340
10 Morris.Thomas, M.T., Irvin, R.J., Thiagarajan, K.P.: 'An investigation into the hydrodynamic efficiency of an oscillating water column', *Journal of Offshore Mechanics and Arctic Engineering*, 2007, **129**, (4), pp. 273–278
11 López, I., Iglesias, G.: 'Efficiency of OWC wave energy converters: A virtual laboratory', *Applied Ocean Research*, 2014, **44**, pp. 63–70
12 Falcão, A.F.d.O., Henriques, J.C.C., Gato, L.M.C.: 'Air turbine optimization for a bottom-standing oscillating-water-column wave energy converter', *Journal of Ocean Engineering and Marine Energy*, 2016, **2**, (4), pp. 459–472
13 He, F., Leng, J., Zhao, X.: 'An experimental investigation into the wave power extraction of a floating box-type breakwater with dual pneumatic chambers', *Applied Ocean Research*, 2017, **67**, pp. 21–30

© The Institution of Engineering and Technology 2015

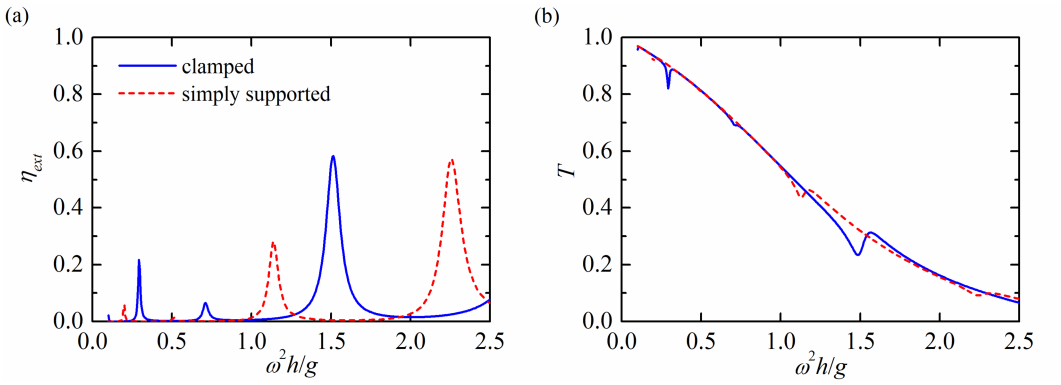

Fig. 7: Frequency response of the wave power absorption efficiency and wave transmission coefficient for different edge conditions, $l_0/h = 0.5$, $d_0/h = 0.5$, $l/h = 1.0$, $d/h = 0.2$, $\bar{\chi} = \chi/h^4 = 4.78 \times 10^{-7}$, $\bar{\gamma} = \gamma/h = 1.258 \times 10^{-3}$, $\beta = 0.24$ and $\bar{\zeta} = \zeta\sqrt{g/h} = 1.0$: (a) η_{ext}; (b) T.

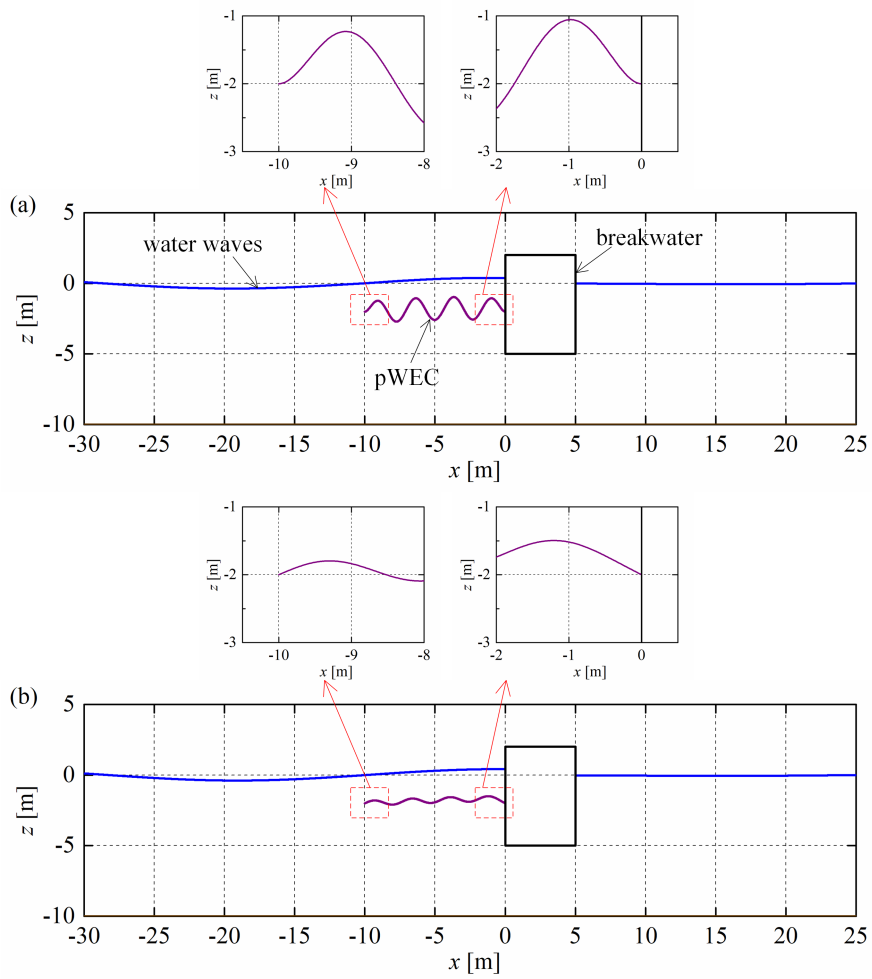

Fig. 8: Snapshot of the free-surface elevation and plate displacement at $t = 0$, $A = 0.2$ m, $h = 10$ m, $\omega^2 h/g = 1.61$ (wave period = 5 s), $l_0/h = 0.5$, $d_0/h = 0.5$, $l/h = 1.0$, $d/h = 0.2$, $\bar{\chi} = \chi/h^4 = 4.78 \times 10^{-7}$, $\bar{\gamma} = \gamma/h = 1.258 \times 10^{-3}$, $\beta = 0.24$ and $\bar{\zeta} = \zeta\sqrt{g/h} = 1.0$: (a) clamped edge; (b) simply supported edge.

14 Pawitan, K.A., Vicinanza, D., Allsop, W., Bruce, T.: 'Front wall and in-chamber impact loads on a breakwater-integrated oscillating water column', *Journal of Waterway, Port, Coastal, and Ocean Engineering*, 2020, **146**, (5), pp. 04020037

15 Zheng, S., Zhu, G., Simmonds, D., Greaves, D., Iglesias, G.: 'Wave power extraction from a tubular structure integrated oscillating water column', *Renewable Energy*, 2020, **150**, pp. 342–355

16 Liu, Z., Xu, C., Kim, K.: 'Overall performance of a model owc system under the free-spinning mode: An experimental study', *Ocean Engineering*, 2021, **227**, pp. 108890

17 Vicinanza, D., Contestabile, P., Quvang Harck Nørgaard, J., Lykke Andersen, T.: 'Innovative rubble mound breakwaters for overtopping wave energy conversion', *Coastal Engineering*, 2014, **88**, pp. 154–170

18 Contestabile, P., Iuppa, C., Di Lauro, E., Cavallaro, L., Andersen, T.L., Vicinanza, D.: 'Wave loadings acting on innovative rubble mound breakwater for overtopping wave energy conversion', *Coastal Engineering*, 2017, **122**, pp. 60–74

19 Musa, M.A., Maliki, A.Y., Ahmad, M.F., Sani, W.N., Yaakob, O., Samo, K.B.: 'Numerical simulation of wave flow over the overtopping breakwater for energy conversion (obrec) device', *Procedia Engineering*, 2017, **194**, pp. 166–173. 10th International Conference on Marine Technology, MARTEC 2016

20 Di Lauro, E., Maza, M., Lara, J.L., Losada, I.J., Contestabile, P., Vicinanza, D.: 'Advantages of an innovative vertical breakwater with an overtopping wave energy converter', *Coastal Engineering*, 2020, **159**, pp. 103713

© The Institution of Engineering and Technology 2015

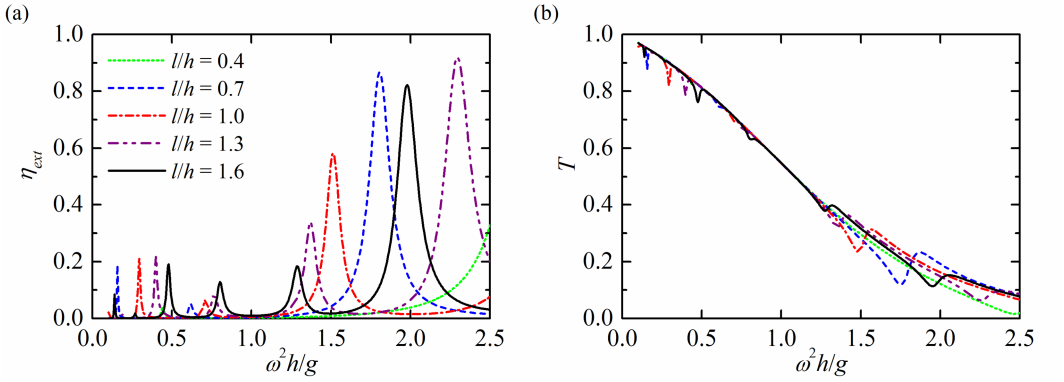

Fig. 9: Frequency response of the wave power absorption efficiency and wave transmission coefficient for different plate widths, $l_0/h = 0.5$, $d_0/h = 0.5$, $d/h = 0.2$, $\bar{\chi} = \chi/h^4 = 4.78 \times 10^{-7}$, $\bar{\gamma} = \gamma/h = 1.258 \times 10^{-3}$, $\beta = 0.24$ and $\bar{\zeta} = \zeta\sqrt{g/h} = 1.0$: (a) η_{ext}; (b) T.

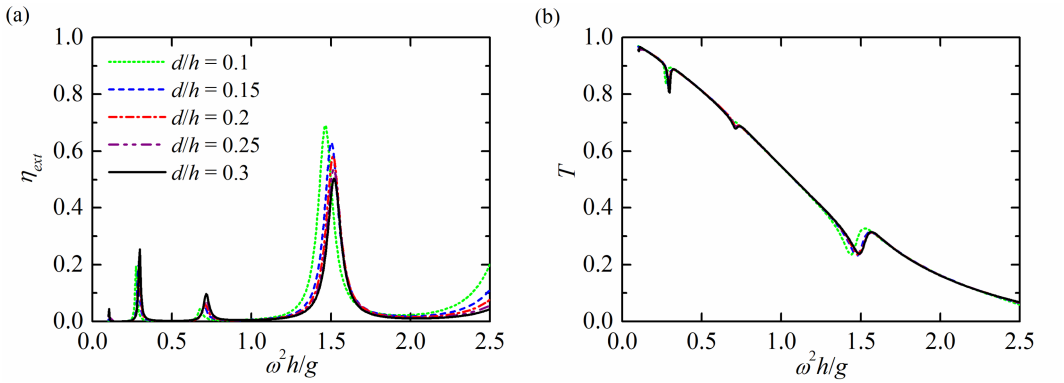

Fig. 10: Frequency response of the wave power absorption efficiency and wave transmission coefficient for different plate submergence, $l_0/h = 0.5$, $d_0/h = 0.5$, $l/h = 1.0$, $\bar{\chi} = \chi/h^4 = 4.78 \times 10^{-7}$, $\bar{\gamma} = \gamma/h = 1.258 \times 10^{-3}$, $\beta = 0.24$ and $\bar{\zeta} = \zeta\sqrt{g/h} = 1.0$: (a) η_{ext}; (b) T.

21 Contestabile, P., Crispino, G., Di Lauro, E., Ferrante, V., Gisonni, C., Vicinanza, D.: 'Overtopping breakwater for wave energy conversion: Review of state of art, recent advancements and what lies ahead', *Renewable Energy*, 2020, **147**, pp. 705–718

22 Schay, J., Bhattacharjee, J., Guedes.Soares, C. 'Numerical modelling of a heaving point absorber in front of a vertical wall'. In: ASME 2013 32nd International Conference on Ocean, Offshore and Arctic Engineering, June 9–14, 2013, Nantes, France. (American Society of Mechanical Engineers Digital Collection, 2013.

23 Ning, D., Zhao, X., Göteman, M., Kang, H.: 'Hydrodynamic performance of a pile-restrained wec-type floating breakwater: An experimental study', *Renewable Energy*, 2016, **95**, pp. 531–541

24 Ning, D.Z., Zhao, X.L., Chen, L.F., Zhao, M.: 'Hydrodynamic performance of an array of wave energy converters integrated with a pontoon-type breakwater', *Energies*, 2018, **11**, (3)

25 Zhao, X.L., Ning, D.Z., Liang, D.F.: 'Experimental investigation on hydrodynamic performance of a breakwater-integrated wec system', *Ocean Engineering*, 2019, **171**, pp. 25–32

26 Konispoliatis, D.N., Mavrakos, S.A.: 'Wave power absorption by arrays of wave energy converters in front of a vertical breakwater: A theoretical study', *Energies*, 2020, **13**, (8)

27 Zhang, C., Ning, D.: 'Hydrodynamic study of a novel breakwater with parabolic openings for wave energy harvest', *Ocean Engineering*, 2019, **182**, pp. 540 – 551

28 Renzi, E.: 'Hydroelectromechanical modelling of a piezoelectric wave energy converter', *Proceedings of the Royal Society A: Mathematical, Physical and Engineering Sciences*, 2016, **472**, pp. 20160715

29 Farley, F.J.M., Rainey, R.C.T., Chaplin, J.R.: 'Rubber tubes in the sea', *Philosophical Transactions of the Royal Society A: Mathematical, Physical and Engineering Sciences*, 2012, **370**, (1959), pp. 381–402

30 Zheng, S., Meylan, M.H., Zhu, G., Greaves, D., Iglesias, G.: 'Hydroelastic interaction between water waves and an array of circular floating porous elastic plates', *Journal of Fluid Mechanics*, 2020, **900**, pp. A20

31 Zheng, S., Meylan, M.H., Greaves, D., Iglesias, G.: 'Water-wave interaction with submerged porous elastic disks', *Physics of Fluids*, 2020, **32**, (4), pp. 047106

32 Behera, H., Sahoo, T.: 'Hydroelastic analysis of gravity wave interaction with submerged horizontal flexible porous plate', *Journal of Fluids and Structures*, 2015, **54**, pp. 643–660

33 Selvan, S.A., Behera, H.: 'Wave energy dissipation by a floating circular flexible porous membrane in single and two-layer fluids', *Ocean Engineering*, 2020, **206**, pp. 107374

34 Zheng, S., Greaves, D., Meylan, M.H., Iglesias, G. 'Wave power extraction by a submerged piezoelectric plate'. In: Developments in Renewable Energies Offshore: Proceedings of the 4th International Conference on Renewable Energies Offshore (RENEW 2020, 12-15 October 2020, Lisbon, Portugal). (CRC Press, 2020. p. 149

35 Buriani, F., Renzi, E. 'Hydrodynamics of a flexible piezoelectric wave energy harvester moored on a breakwater'. In: 12th European Wave and Tidal Energy Conference (EWTEC). (Cork, Ireland, 2017.

36 Athanassoulis, G.A., Mamis, K.I.: 'Modeling and analysis of a cliff-mounted piezoelectric sea-wave energy absorption system', *Coupled Systems Mechanics*, 2013, **2**, (1), pp. 53–83

37 Liu, C., Huang, Z.: 'A flexible membrane breakwater with a piezoelectric layer for providing harborage and wave-energy conversion', *Journal of Coastal Research*, 2019, **36**, (1), pp. 148 – 156

38 Buriani, F. 'Mathematical modelling of wave–structure interactions with application to wave energy conversion'. Loughborough University, 2019

39 Zheng, S., Zhang, Y.: 'Wave diffraction and radiation by multiple rectangular floaters', *Journal of Hydraulic Research*, 2016, **54**, (1), pp. 102–115

40 Zheng, S., Zhang, Y.: 'Analytical study on wave power extraction from a hybrid wave energy converter', *Ocean Engineering*, 2018, **165**, pp. 252–263

41 Mahmood.Ul.Hassan, Meylan, M.H., Peter, M.A.: 'Water-wave scattering by submerged elastic plates', *The Quarterly Journal of Mechanics and Applied Mathematics*, 2009, **62**, (3), pp. 321–344

42 Meylan, M.H., Bennetts, L.G., Peter, M.A.: 'Water-wave scattering and energy dissipation by a floating porous elastic plate in three dimensions', *Wave Motion*, 2017, **70**, pp. 240–250

43 Zheng, S., Meylan, M.H., Fan, L., Greaves, D., Iglesias, G.: 'Wave scattering by a floating porous elastic plate of arbitrary shape: a semi-analytical study', *Journal of Fluids and Structures*, 2020, **92**, pp. 102827

44 Wu, J., Wan, Z., Fang, Y.: 'Wave reflection by a vertical wall with a horizontal submerged porous plate', *Ocean Engineering*, 1998, **25**, (9), pp. 767 – 779

45 Farina, L., da Gama, R.L., Korotov, S., Ziebell, J.S.: 'Radiation of water waves by a submerged nearly circular plate', *Journal of Computational and Applied Mathematics*, 2017, **310**, pp. 165–173

© The Institution of Engineering and Technology 2015

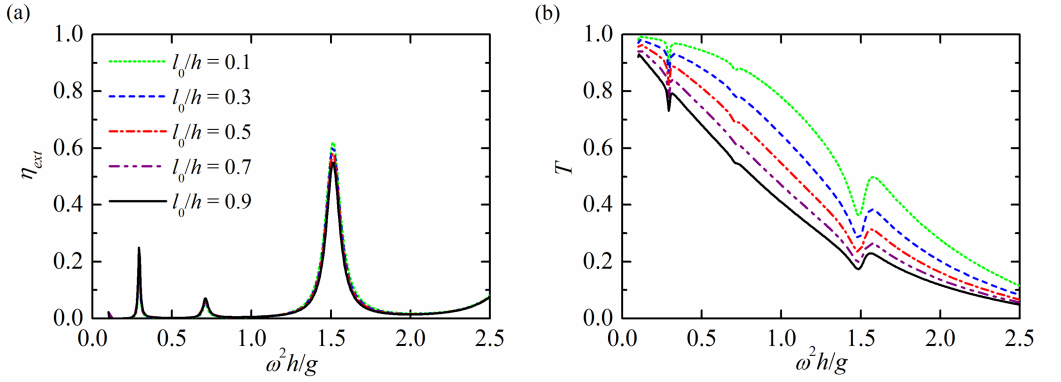

Fig. 11: Frequency response of the wave power absorption efficiency and wave transmission coefficient for different breakwater widths, $d_0/h = 0.5$, $l/h = 1.0$, $d/h = 0.2$, $\bar{\chi} = \chi/h^4 = 4.78 \times 10^{-7}$, $\bar{\gamma} = \gamma/h = 1.258 \times 10^{-3}$, $\beta = 0.24$ and $\bar{\zeta} = \zeta\sqrt{g/h} = 1.0$: (a) η_{ext}; (b) T.

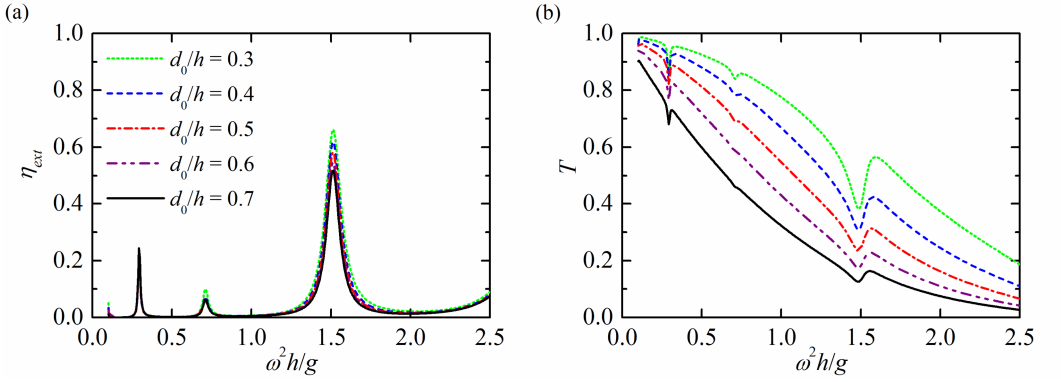

Fig. 12: Frequency response of the wave power absorption efficiency and wave transmission coefficient for different breakwater drafts, $l_0/h = 0.5$, $l/h = 1.0$, $d/h = 0.2$, $\bar{\chi} = \chi/h^4 = 4.78 \times 10^{-7}$, $\bar{\gamma} = \gamma/h = 1.258 \times 10^{-3}$, $\beta = 0.24$ and $\bar{\zeta} = \zeta\sqrt{g/h} = 1.0$: (a) η_{ext}; (b) T.

8 Appendix Derivation process of the formulas and calculation for the unknown coefficients A_n, B_n, C_n, D_n, E_n and F_n

Here we take the case with simply supported edge condition as an example to show how to determine the unknown coefficients A_n, B_n, C_n, D_n, E_n and F_n. Inserting the expression of the spatial potentials at different regions of the fluid domain, i.e., Eqs. (14), (17), (18) and (21), into the continuity conditions, which should be satisfied at the interfaces between each two adjacent regions, and the simply supported edge boundary conditions, i.e., Eqs. (22)-(27) and (12), gives:

$$-\frac{\mathrm{i}gA}{\omega}\mathrm{e}^{-\mathrm{i}kl}Z_0(z) + \sum_{n=0}^{\infty} A_n \mathrm{e}^{\mathrm{i}k_n l} Z_n(z)$$
$$= \sum_{n=-2}^{\infty} (C_n \mathrm{e}^{-\kappa_n l} + D_n \mathrm{e}^{\kappa_n l}) Y_n(z), \quad z \in [-h, 0], \tag{38}$$

$$\sum_{n=-2}^{\infty} (C_n + D_n) Y_n(z) = F_0 + \sum_{n=1}^{\infty} (E_n + F_n)$$
$$\times \cos[\beta_n(z+h)], \quad z \in [-h, -d_0], \tag{39}$$

$$E_0 l_0 + F_0 + \sum_{n=1}^{\infty} (E_n \mathrm{e}^{\beta_n l_0} + F_n \mathrm{e}^{-\beta_n l_0}) \times$$
$$\cos[\beta_n(z+h)] = \sum_{n=0}^{\infty} B_n \mathrm{e}^{\mathrm{i}k_n l_0} Z_n(z), \quad z \in [-h, -d_0], \tag{40}$$

$$\frac{kgA}{\omega}\mathrm{e}^{-\mathrm{i}kl}Z_0(z) - \mathrm{i}\sum_{n=0}^{\infty} k_n A_n \mathrm{e}^{\mathrm{i}k_n l} Z_n(z)$$
$$= \sum_{n=-2}^{\infty} \kappa_n (C_n \mathrm{e}^{-\kappa_n l} - D_n \mathrm{e}^{\kappa_n l}) Y_n(z), \quad z \in [-h, 0], \tag{41}$$

$$\sum_{n=-2}^{\infty} \kappa_n (C_n - D_n) Y_n(z)$$
$$= \begin{cases} 0, & z \in [-d_0, 0], \\ E_0 + \sum_{n=1}^{\infty} \beta_n (E_n - F_n) \cos[\beta_n(z+h)], & z \in [-h, -d_0]. \end{cases} \tag{42}$$

$$\mathrm{i}\sum_{n=0}^{\infty} k_n B_n \mathrm{e}^{\mathrm{i}k_n l_0} Z_n(z)$$
$$= \begin{cases} 0, & z \in [-d_0, 0], \\ E_0 + \sum_{n=1}^{\infty} \beta_n (E_n \mathrm{e}^{\beta_n l_0} - F_n \mathrm{e}^{-\beta_n l_0}) \cos[\beta_n(z+h)], & z \in [-h, -d_0]. \end{cases} \tag{43}$$

© The Institution of Engineering and Technology 2015

Table 1 Multiplying terms and the corresponding intervals of integration for Eqs. (38)-(43).

Equation	(38)	(39)	(40)	(41)	(42)	(43)
multiplying term	$Z_\tau(z)$	$\cos[\beta_\tau(z+h)]$	$\cos[\beta_\tau(z+h)]$	$Z_\tau(z)$	$Z_\tau(z)$	$Z_\tau(z)$
interval of integration	$[-h,0]$	$[-h,-d_0]$	$[-h,-d_0]$	$[-h,0]$	$[-h,0]$	$[-h,0]$

$$\sum_{n=-2}^{\infty}\kappa_n\sin(\kappa_n c)\big[\kappa_n h\sin(\kappa_n d)+\frac{\omega^2}{g}h\cos(\kappa_n d)\big]\times(C_n\mathrm{e}^{-\kappa_n l}+D_n\mathrm{e}^{\kappa_n l})=0, \quad (44)$$

$$\sum_{n=-2}^{\infty}\kappa_n\sin(\kappa_n c)\big[\kappa_n h\sin(\kappa_n d)+\frac{\omega^2}{g}h\cos(\kappa_n d)\big]\times(C_n+D_n)=0, \quad (45)$$

$$\sum_{n=-2}^{\infty}\kappa_n^3\sin(\kappa_n c)\big[\kappa_n h\sin(\kappa_n d)+\frac{\omega^2}{g}h\cos(\kappa_n d)\big]\times(C_n\mathrm{e}^{-\kappa_n l}+D_n\mathrm{e}^{\kappa_n l})=0, \quad (46)$$

$$\sum_{n=-2}^{\infty}\kappa_n^3\sin(\kappa_n c)\big[\kappa_n h\sin(\kappa_n d)+\frac{\omega^2}{g}h\cos(\kappa_n d)\big]\times(C_n+D_n)=0. \quad (47)$$

If the plate is clamped at its edge, then Eqs. (46) and (47) should be replaced by

$$\sum_{n=-2}^{\infty}\kappa_n^2\sin(\kappa_n c)\big[\kappa_n h\sin(\kappa_n d)+\frac{\omega^2}{g}h\cos(\kappa_n d)\big]\times(C_n\mathrm{e}^{-\kappa_n l}-D_n\mathrm{e}^{\kappa_n l})=0, \quad (48)$$

and

$$\sum_{n=-2}^{\infty}\kappa_n^2\sin(\kappa_n c)\big[\kappa_n h\sin(\kappa_n d)+\frac{\omega^2}{g}h\cos(\kappa_n d)\big]\times(C_n-D_n)=0. \quad (49)$$

The orthonormal properties of $Z_n(z)$ and $\cos[\beta_n(z+h)]$ can be used to help determine the unknown coefficients. Table 1 lists the multiplying terms and the corresponding intervals of integration for Eqs. (38)-(43).

After multiplying both sides of each equation among Eqs. (38)-(43) with the corresponding listed term, integrating vertically over the listed interval, and making some rearrangement, Eqs. (38)-(43) can be rewritten as

$$A_\tau\mathrm{e}^{\mathrm{i}k_\tau l}H_\tau^{(1)}-\sum_{n=-2}^{\infty}(C_n\mathrm{e}^{-\kappa_n l}+D_n\mathrm{e}^{\kappa_n l})J_{n,\tau}^{(1)}=\delta_{0,\tau}\frac{\mathrm{i}gA}{\omega}\mathrm{e}^{-\mathrm{i}kl}H_0^{(1)}, \quad (50)$$

$$\sum_{n=-2}^{\infty}(C_n+D_n)J_{n,\tau}^{(2)}-\delta_{0,\tau}F_0H_\tau^{(2)}-(1-\delta_{0,\tau})(E_\tau+F_\tau)H_\tau^{(2)}=0, \quad (51)$$

$$\sum_{n=0}^{\infty}B_n\mathrm{e}^{\mathrm{i}k_n l_0}J_{n,\tau}^{(3)}-\delta_{0,\tau}(E_0l_0+F_0)H_\tau^{(2)}-(1-\delta_{0,\tau})(E_\tau\mathrm{e}^{\beta_\tau l_0}+F_\tau\mathrm{e}^{-\beta_\tau l_0})H_\tau^{(2)}=0, \quad (52)$$

$$\mathrm{i}k_\tau A_\tau\mathrm{e}^{\mathrm{i}k_\tau l}H_\tau^{(1)}+\sum_{n=-2}^{\infty}\kappa_n(C_n\mathrm{e}^{-\kappa_n l}-D_n\mathrm{e}^{\kappa_n l})J_{n,\tau}^{(1)}=\delta_{0,\tau}\frac{kgA}{\omega}\mathrm{e}^{-\mathrm{i}kl}H_0^{(1)}, \quad (53)$$

$$\sum_{n=-2}^{\infty}\kappa_n(C_n-D_n)J_{n,\tau}^{(1)}-E_0J_{\tau,0}^{(3)}-\sum_{n=1}^{\infty}\beta_n(E_n-F_n)J_{\tau,n}^{(3)}=0, \quad (54)$$

$$\mathrm{i}k_\tau B_\tau\mathrm{e}^{\mathrm{i}k_\tau l_0}H_\tau^{(1)}-E_0J_{\tau,0}^{(3)}-\sum_{n=1}^{\infty}\beta_n(E_n\mathrm{e}^{\beta_n l_0}-F_n\mathrm{e}^{-\beta_n l_0})J_{\tau,n}^{(3)}=0, \quad (55)$$

where

$$H_n^{(1)}=\int_{-h}^{0}Z_n^2(z)\,\mathrm{d}z=\frac{\sinh(k_nh)\cosh(k_nh)+k_lh}{2k_n\cosh^2(k_nh)}, \quad (56)$$

$$H_n^{(2)}=\int_{-h}^{-d_0}\cos^2[\beta_n(z+h)]\,\mathrm{d}z=\begin{cases}h-d_0, & n=0\\ \frac{h-d_0}{2}, & n=1,2,\cdots\end{cases}, \quad (57)$$

$$J_{n,\tau}^{(1)}=\int_{-h}^{0}Y_n(z)Z_\tau(z)\,\mathrm{d}z=\frac{k_\tau h\sinh(k_\tau c)\big[\frac{\omega^2}{g}\cos(\kappa_n h)+\kappa_n\sin(\kappa_n h)\big]}{\cosh(k_\tau h)\big(\kappa_n^2+k_\tau^2\big)}, \quad (58)$$

$$J_{n,\tau}^{(2)}=\int_{-h}^{-d_0}Y_n(z)\cos[\beta_\tau(z+h)]\,\mathrm{d}z=\left[\kappa_n h\sin(\kappa_n d)+\frac{\omega^2h}{g}\cos(\kappa_n d)\right]\times\frac{\kappa_n(h-d_0)^2(-1)^\tau\sin[\kappa_n(h-d_0)]}{(h-d_0)^2\kappa_n^2-\tau^2\pi^2}, \quad (59)$$

$$J_{n,\tau}^{(3)}=\int_{-h}^{-d_0}Z_n(z)\cos[\beta_\tau(z+h)]\,\mathrm{d}z=\frac{(h-d_0)^2(-1)^\tau k_n\sinh[k_n(h-d_0)]}{[(h-d_0)^2k_n^2+\tau^2\pi^2]\cosh(k_nh)}. \quad (60)$$

To evaluate the unknown coefficients A_n, B_n, C_n, D_n, E_n and F_n, we truncate all infinite series of vertical eigenfunctions at N,

© The Institution of Engineering and Technology 2015

i.e., $(N+1)$ terms $(n = 0,\ 1,\ \cdots,\ N)$ for A_n, B_n, E_n and F_n and $(N+3)$ terms $(n = -2,\ -1,\ 0,\ 1,\ \cdots,\ N)$ for C_n and D_n, resulting in $(6N+10)$ unknown coefficients to be determined. After taking $(\tau = 0,\ 1,\ \cdots,\ N)$ in Eqs. (50)-(55) and with the simply supported edge conditions Eqs. (44)-(47) appended, a $(6N+10)$ order complex linear equation matrix is obtained, which can be used to determine the exact same number of unknown coefficients. N should be chosen large enough to lead to accurate results. In all the theoretical computations as given in this paper, $N = 40$ are used, unless otherwise specified. It should be noted that Eqs. (50), (53), and (54) with $J^{(3)}_{\tau,n}$ for $n = 0,\ 1,\ 2, \cdots$ replaced by 0, together with Eqs. (44)-(47), are the equations which can be used to solve the wave diffraction problem of a pizoelectric WEC submerged in front of a bottom-seated breakwater [35].

© The Institution of Engineering and Technology 2015